

Zeeman spin splittings in semiconductor nanostructures

R. Kotlyar and T. L. Reinecke

Naval Research Laboratory, Washington, D.C. 20375

M. Bayer and A. Forchel

Technische Physik, Universität Würzburg, Am Hubland, D 97074 Würzburg, Germany

(Received 18 October 2000; published 2 February 2001)

A systematic theoretical and experimental study of Zeeman spin splittings and g factors in semiconductor nanostructures is given. Six-band effective-mass calculations of electron, hole, and exciton spin splittings are made and are shown to account for experimental results presented here on $\text{In}_{0.10}\text{Ga}_{0.90}\text{As}/\text{GaAs}$ systems for the size dependences of g factors in deep-etched quantum dots and wires and for the magnetic-field dependences of the Zeeman splittings in quantum wells. These effects are traced to band mixing, and an analytic form of the results is given that connects these two effects and describes their dependences on dimensionality.

DOI: 10.1103/PhysRevB.63.085310

PACS number(s): 73.21.-b, 73.22.-f, 71.35.Ji

During the past decade there has been intense interest in understanding and exploiting the properties of the charge degrees of freedom of carriers in semiconductor nanostructures (quantum wells, quantum wires, and quantum dots). Recently, their spin degrees of freedom have begun to attract considerable interest both for their physical properties and also in connection with several issues involving applications. For example, in “spin electronics” one seeks to use the spin densities in place of charges in a range of systems such as spin transistors and light-emitting diodes. Very recently interest in spin effects has been spurred by the observation of long spin-coherence times in semiconductors and in their nanostructures,¹ which make solid state implementations for quantum information processing attractive. Examples include recent proposals for implementations for quantum computation using spins in quantum dots^{2,3} and spins in heterostructures.⁴ In all of these issues the ability to enhance and control spin splittings in semiconductors plays a key role.

Recent advances in the understanding of spin effects in the optical properties of nanostructures includes work on their exciton Zeeman spin splittings,⁵ on the smaller electron-hole exchange splittings, which have been studied in some detail,^{6,7} on spin-dependent relaxation and on exciton “dark states,”⁸ and even on the hyperfine interaction of electron spins with nuclear spins.⁶

The key quantity needed in understanding spin effects in optical properties is the Zeeman splitting in a magnetic field. The splitting is determined by mixing of the spin with the electronic states. Thus, the splitting not only controls the magnitude of spin effects, but also can give important insight into relaxation and coherence through the coupling of the spin to electronic and lattice degrees of freedom. To date, however, results for the Zeeman splittings and the associated g factors have been only fragmentary, and they remain poorly understood in these systems. Some experimental results^{9–12} and some calculations^{11–13} have been given for quantum wells. Experimental results^{5,14} have been given for some quantum dots, and some calculations have been made within approximations for conduction-band electrons in quantum wires and dots.¹³

Experimental results have been reported for two features that give critical tests of our understanding of Zeeman splittings in nanostructures. (i) In quantum dots the Zeeman splittings of excitons are approximately linear in B , but the associated g factors depend strongly on the structure size.¹⁴ (ii) Exciton Zeeman splittings in quantum wells have strong (well-width-dependent) nonlinear dependences on the magnetic field B , even becoming negative in narrow wells.^{9,12} In order to understand these effects, reliable theoretical results are needed for realistic systems including the full band couplings, and comparisons need to be made with accurate experimental results for systems where the parameters (size, shape, alloy concentration, potentials) are known sufficiently well.¹⁵

Here a full six-band treatment of the electron and hole Zeeman splittings and g factors for realistic quantum wells, quantum wires, and quantum dots is given. These results provide an explanation of the dependences on quantum dot and quantum wire size and on magnetic field previously reported. We also obtain an accurate perturbative form for spin splittings in nanostructures and use it to establish in a simple and intuitive way the connections between the size and magnetic-field dependences in zero, one, and two dimensions (wells, wires, and dots). We give here experimental results for these features from photoluminescence studies on $\text{InGaAs}/\text{GaAs}$ quantum wells and deep-etched $\text{InGaAs}/\text{GaAs}$ quantum dots and quantum wires with widely varying sizes. These systems have fairly well characterized structures and potentials, and more importantly their sizes and dimensionality vary widely and systematically. This permits a definitive comparison to be made here between theory and experiment.

A standard six-band $\mathbf{k}\cdot\mathbf{p}$ effective-mass Kane-Luttinger Hamiltonian of the band-edge carrier states in III-V semiconductors is used,¹⁶ which includes the coupling of the light-hole and heavy-hole valence bands and also their coupling with the conduction band. The split-off spin-orbit band is removed in energy in these materials and is included perturbatively in the parameters. For the quantum wells, the conduction- and valence-band offsets at the interface between GaAs and $\text{In}_{0.10}\text{Ga}_{0.90}\text{As}$ are taken to be 79.9 and 69.2

meV, respectively.¹⁰ The g factors of the electrons and holes in the Hamiltonian are chosen by weighting the bulk values with the quantum well ground wave functions ζ_0^j :¹³ $g_j^{\text{well}} = g_j^{\text{GaAs}} \int_{|z|>l_z/2} |\zeta_0^j(z)|^2 dz + g_j^{\text{InGaAs}} \int_{|z|<l_z/2} |\zeta_0^j(z)|^2 dz$, where g_j^{GaAs} and g_j^{InGaAs} are the bulk g factors for the j th electron or hole band. A splitting of 40 meV between the light- and heavy-hole bands is included to account for the strain due to lattice mismatch at the interface; it is in accord with experiment for quantum wells. The magnetic field is taken to be in the growth direction (z). The electron and hole functions in the quantum well with zero magnetic field are taken to have the form $\{Z_1(z), Z_2(z), Z_3(z), Z_4(z), Z_5(z), Z_6(z)\}$, where the first two components refer to electrons with spin up and spin down, and the last four are for the heavy holes and light holes with total angular momentum $\frac{3}{2}$.¹⁶ $Z_j(z)$, $j = 1, \dots, 6$, are expanded as $Z_j(z) = \sum_l a_l^j \zeta_l^j(z)$ in quantum well subband functions ζ_l^j corresponding to the diagonal terms in the Hamiltonian, i.e., without band mixing. These six functions in the quantum well at $B=0$ are multiplied by the corresponding radial functions from the Luttinger-Landau set of harmonic oscillator functions at nonzero field in the bulk case.¹⁷

For realistic quantum dots and quantum wires, direct numerical evaluations of the g factors generally require the expansion of the wave functions in large basis sets and the diagonalization of very large Hamiltonian matrices. In order to overcome this, we have developed a perturbative approach for these low-dimensional systems. The Hamiltonian is written for the quantum well as a term $H_0(k_{\parallel}=0)$ for zero parallel wave vector k_{\parallel} plus $H_1 = (\hbar^2/2m_0)[\hat{O}_+ k_+ + \hat{O}_- k_- + \hat{O}_{2+} k_+^2 + \hat{O}_{2-} k_-^2]$, where the matrices \hat{O}_i , $i = +, -, 2+,$ and $2-$, are read directly from the Hamiltonian, and $k_{\pm} = k_x \pm ik_y$. Treating H_1 perturbatively, we write the dispersion of an electron or hole (i) in the quantum well plane up to order k_{\parallel}^2 as

$$E_i(k_{\parallel}) = E_i(k_{\parallel}=0) + \frac{\hbar^2 k_{\parallel}^2}{2m_{\text{eff},\parallel}^i} + \frac{\mu_0 B}{2} [g_0^i + g_{20}^i + (g_{22}^i + g_{32}^i + g_{42}^i) k_{\parallel}^2], \quad (1)$$

where the first index of each of the g_{ij} labels the order of perturbation theory, and the second the power of k_{\parallel} .

From Eq. (1) contributions up to fourth order in perturbation theory are needed to describe the g factors. Equation (1) gives the carrier dispersion in terms of an effective mass

$$(m_{\text{eff},\parallel}^i)^{-1} = m_0^{-1} \left[\left\langle i \left| \frac{m_0}{m_{\parallel}^*} \right| i \right\rangle + \Delta_-^{(2)} + \Delta_+^{(2)} \right]$$

and coefficients of magnetic field B given by

$$\begin{aligned} g_0^i &= \langle i | g_0 | i \rangle, & g_{20}^i &= 2(\Delta_-^{(2)} - \Delta_+^{(2)}), \\ g_{22}^i &= 8(\Delta_{2-}^{(2)} - \Delta_{2+}^{(2)}), & g_{42}^i &= g_{42,1}^i - g_{42,2}^i, \\ g_{32}^i &= 8(\Delta_{2++}^{(3)} + \Delta_{2--}^{(3)} - \Delta_{2+-}^{(3)} - \Delta_{2-+}^{(3)}), \end{aligned}$$

$$\begin{aligned} g_{42,1}^i &= 4(2\Delta_{-++}^{(4,1)} + \Delta_{-+-}^{(4,1)} - 2\Delta_{+--}^{(4,1)} - \Delta_{+-+}^{(4,1)}), \\ g_{42,2}^i &= 4(2\Delta_{-++}^{(4,2)} + \Delta_{-+-}^{(4,2)} - 2\Delta_{+--}^{(4,2)} - \Delta_{+-+}^{(4,2)}), \\ g_{42,2}^i &= 4(2\Delta_{-++}^{(4,2)} + \Delta_{-+-}^{(4,2)} - 2\Delta_{+--}^{(4,2)} - \Delta_{+-+}^{(4,2)}). \end{aligned} \quad (2)$$

The Δ 's are expressed in perturbation theory by

$$\begin{aligned} \Delta_{\alpha}^{(2)} &= \sum_{p \neq i} \frac{[\hbar^2/2m_0](\hat{O}_{\alpha})_{ip}^2}{(E_i^{(0)} - E_p^{(0)})}, \\ \Delta_{\alpha\beta\gamma}^{(3)} &= \sum_{p', p'' \neq i} \frac{[\hbar^2/2m_0]^2 (\hat{O}_{\alpha})_{ip'} (\hat{O}_{\beta})_{p'p''} (\hat{O}_{\gamma})_{p''i}}{(E_i^{(0)} - E_{p'}^{(0)})(E_i^{(0)} - E_{p''}^{(0)})}, \\ \Delta_{\alpha\beta\gamma\delta}^{(4,1)} &= \sum_{p'', p', p \neq i} \frac{[\hbar^2/2m_0]^3 (\hat{O}_{\alpha})_{ip''} (\hat{O}_{\beta})_{p''p'} (\hat{O}_{\gamma})_{p'p} (\hat{O}_{\delta})_{pi}}{(E_i^{(0)} - E_{p''}^{(0)})(E_i^{(0)} - E_{p'}^{(0)})(E_i^{(0)} - E_p^{(0)})}, \\ \Delta_{\alpha\beta\gamma\delta}^{(4,2)} &= \sum_{p', p \neq i} \frac{[\hbar^2/2m_0]^3 (\hat{O}_{\alpha})_{ip'} (\hat{O}_{\beta})_{ip'} (\hat{O}_{\gamma})_{pi} (\hat{O}_{\delta})_{p'i}}{(E_i^{(0)} - E_{p'}^{(0)})^2 (E_i^{(0)} - E_p^{(0)})}, \end{aligned} \quad (3)$$

where i and p represent the edge states of the electron and hole subbands in the well with zero magnetic field. The perturbative approach in Eq. (1) is applicable to all situations with nondegenerate subbands due to vertical (quantum well) confinement.

Equation (1) is our main theoretical result, and it accounts for the observed size dependences of the g factors in dots^{5,14} and for the observed nonlinearities of the spin splittings with B in quantum wells.^{9,12} The spin splittings are given by the last term in Eq. (1) where the k_{\parallel}^2 terms arise from mixing (through H_1) of the subband states of the quantum well potential. In quantum dots and wires the carrier functions are confined, and the dominant term in $\langle k_{\parallel}^2 \rangle$ at small B is $\langle k_{\parallel}^2 \rangle \sim 1/L^2$, where L is the size. This gives a size dependence to the g factor in quantum dots and wires. In a quantum well in a magnetic field, $\langle k_{\parallel}^2 \rangle \sim \hbar \omega_c \sim B$, where ω_c is the cyclotron frequency. In this case in effect the carrier is ‘‘localized’’ in a Landau state, and then these contributions to the third term in Eq. (1) give nonlinear dependences of the splitting on B . Thus we see that the size dependences in quantum dots and quantum wires and the B dependences in quantum wells are intimately connected through the last term in Eq. (1).

To make quantitative comparisons with experiment, we have made photoluminescence studies of $\text{In}_{0.10}\text{Ga}_{0.90}\text{As}/\text{GaAs}$ quantum well structures grown by molecular beam epitaxy, and of quantum wire and quantum dot structures obtained by deep wet chemical etching of single 5 nm quantum wells. The details of the experiments were given earlier.^{14,18} Typical spectra for arrays of quantum dots of differing diameters at $B=8$ T are given in Fig. 1(b). In Fig. 1(b) [1(a)], to facilitate the comparison of splittings at different dot diameters (well widths), we have aligned the spectra at the origin by subtracting the energy of the center of the spin-split emission lines. The diamagnetic shifts¹⁹ and the

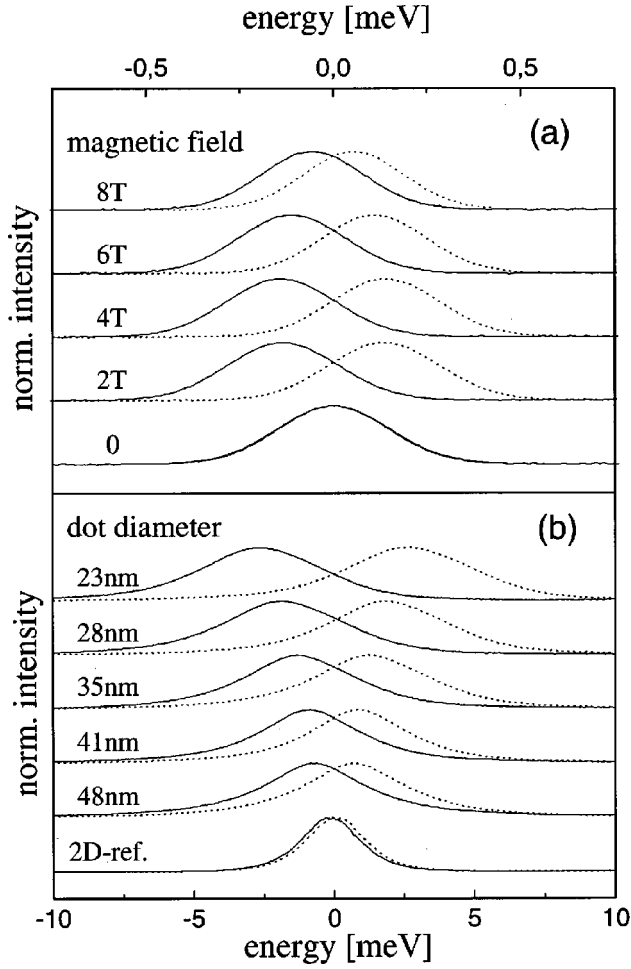


FIG. 1. (a) Photoluminescence spectra of 15 nm $\text{In}_{0.10}\text{Ga}_{0.90}\text{As}/\text{GaAs}$ quantum wells for magnetic fields B indicated. (b) Photoluminescence spectra of arrays of $\text{In}_{0.10}\text{Ga}_{0.90}\text{As}/\text{GaAs}$ deep-etched quantum dots with the sizes indicated at $B=8$ T. Solid lines give σ^+ polarized spectra and dotted lines σ^- spectra. For ease of comparison the peaks of the lines have been shifted to a common energy here. The absolute energy positions of the lines in (b) are (in eV) 1.4592, 1.4571, 1.4558, 1.4536, 1.4534, and 1.4513 for dots of size (in nm) 23, 28, 35, 41, 48, and for the unetched structure.

effects of strain relief^{19,20} in these structures have been discussed previously. In Fig. 1(b) there is a dramatic increase in the exciton spin splitting for decreasing dot size. For the dot and wire systems studied here the spin splittings were found to increase approximately linearly with B within the experimental accuracy, and thus we obtain the exciton g factor from $E(\sigma^+) - E(\sigma^-) = g_{\text{ex}} \mu_B B$. In Fig. 1(a), typical spectra for a 15 nm quantum well are shown as a function of magnetic field B . There the splitting between the two circular polarizations has a strong nonlinear dependence on B : For small B it increases with B and reaches a maximum at 5 T, and for higher fields it decreases again. The B dependences of the splittings for quantum wells of several widths are displayed in Fig. 2. For quantum wires and quantum dots, the resulting g_{ex} are given in Fig. 3 as functions of size.

Detailed theoretical results for the exciton spin splittings

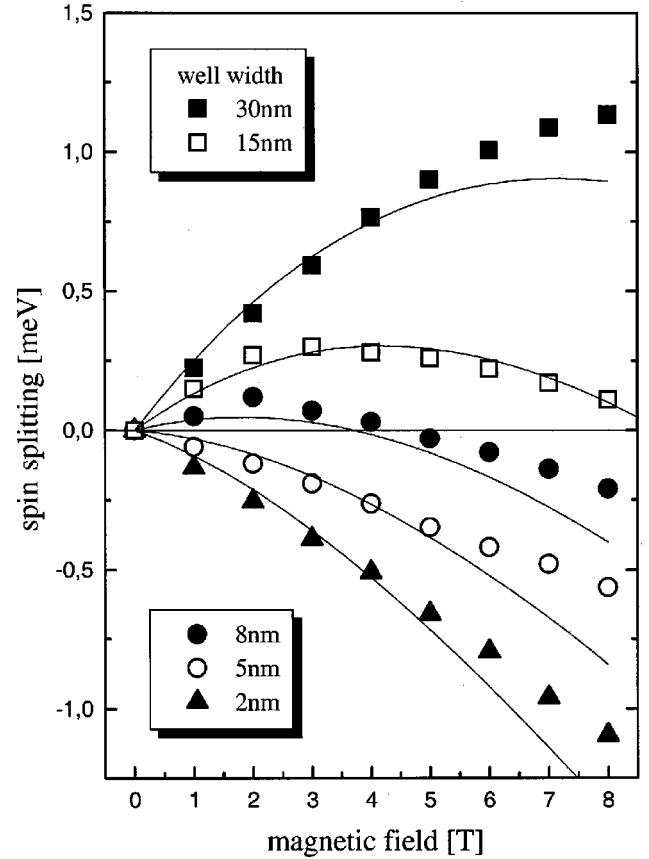


FIG. 2. Experimental spin splittings and theoretical calculations (solid lines) as functions of the magnetic field along the growth direction for varying $\text{In}_{0.10}\text{Ga}_{0.90}\text{As}/\text{GaAs}$ quantum well sizes indicated in the legend.

in $\text{In}_{0.10}\text{Ga}_{0.90}\text{As}/\text{GaAs}$ quantum wells were obtained by diagonalizing the full Hamiltonian directly for nonzero B using the expansion basis discussed above,²¹ and they are shown in Fig. 2. In order to include the quantum well continuum states, the quantum well system is placed in a large one-dimensional box of size L_z with infinite potentials,²² where $L_z/l_z \sim 100-200$ with l_z the width of the quantum well. Convergence was obtained for the spin splittings by using ~ 100 quantum well ζ_l^j functions for each $Z_j(z)$, and the results have been checked for convergence with respect to the size L_z .

The agreement between experiment and theory is good for both the B dependences and the well-width dependences of the quantum well splittings. The spin splittings have nonlinear dependences on B , and for small wells they become negative. The nonlinearities in B arise from the B^2 contributions in the term in Eq. (1) after the evaluation $\langle k_{\parallel}^2 \rangle \sim \hbar \omega_c \sim B$. The coefficients depend on well width and give the width dependence of the splittings. All the perturbation corrections (the terms in g_{j2}^{hh} and g_{20}^{hh}) are negative for the heavy-hole exciton because the dominant contributions are from the light-hole heavy-hole coupling, and they increase in magnitude with decreasing width. This leads to negative splittings in narrow enough wells. Therefore the exciton g factors, which are obtained from the low- B limits of the curves in

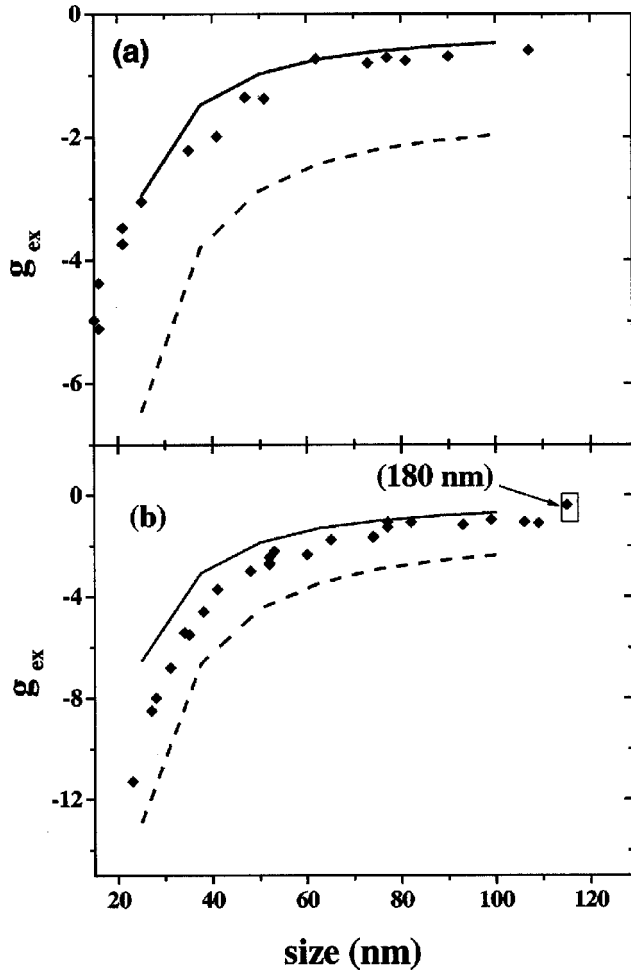


FIG. 3. Size dependences of exciton g factors as functions of (a) quantum wire width and (b) quantum dot diameter. Symbols give experimental results for deep-etched $\text{In}_{0.10}\text{Ga}_{0.90}\text{As}/\text{GaAs}$ wires and dots. Solid curves give calculations made with a 40 meV light-hole/heavy-hole strain splitting, and dashed curves those for zero strain splitting.

Fig. 2, become negative in narrow wells. These results are consistent with experiments which find negative exciton g factors in narrow wells.^{9,12} In particular, we find that the heavy-hole exciton g factors g_{ex} are $-1.46, 0.31, 0.78, 1.31, 2.57,$ and 4.76 for the quantum wells of 2, 5, 8, 15, and 30 nm shown in Fig. 2.

Theoretical results for electron and hole g factors in deep-etched cylindrical quantum dots and rectangular quantum wires are obtained from Eq. (1) by evaluating k_{\parallel} appropriately using the quantum well subband edge states at $B=0$. The potentials at the lateral sides of the deep-etched structures are taken to be infinite. The perturbative approach in Eq. (1) is valid if the lateral confinement energies are smaller than the quantum well confinement energies, as is the case here. For the sizes and fields in Fig. 3, the structure size dependence of $\langle k_{\parallel}^2 \rangle$ is greater than the B dependence. Thus the spin splitting in dots and wires is linear in B , which is in agreement with our experimental results. For larger sizes and fields than those shown here, the B -dependent contributions

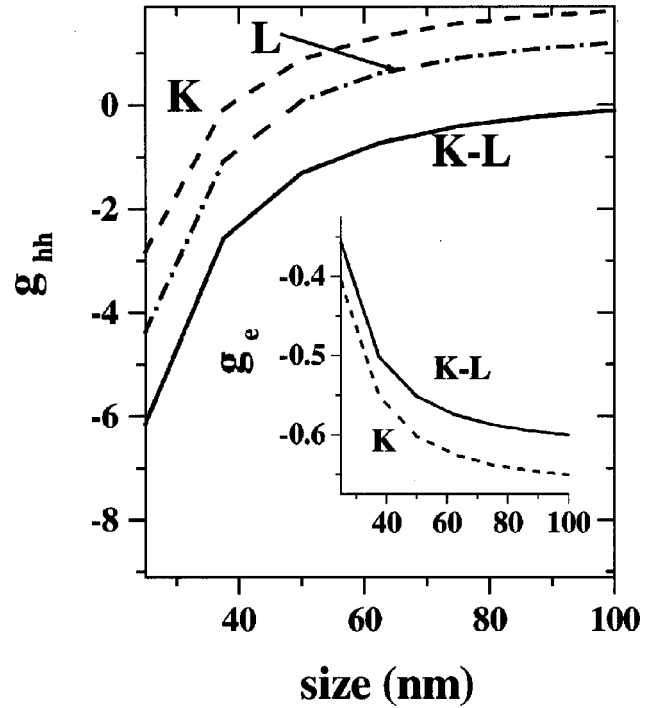


FIG. 4. Calculations of g factors for holes in the dots obtained using different treatments of the band coupling as described in the text: only conduction-hole band coupling (K), only valence-band coupling (L), and both of these couplings (K-L). The inset gives corresponding results for the electrons.

in $\langle k_{\parallel}^2 \rangle$ in the last term in Eq. (1) would become more important, and for large enough size the nonlinear B behavior seen in wells would be recovered.

Electron-hole exchange effects in similar nanostructures typically are much smaller ($<50 \mu\text{eV}$) than the spin splittings studied here.⁶ Thus theoretical values of the exciton g factor can be obtained from our calculations for the electron and the heavy hole by $g_{\text{ex}} = g_e + g_{\text{hh}}$. The resulting theoretical exciton g factors for quantum dots and quantum wires are shown in Fig. 3. The agreement between experiment and theory both for magnitude and for size dependence is good. The absolute values of g_{ex} increase dramatically for decreasing dot and wire sizes. The size dependence is stronger in dots than wires. This difference between dots and wires arises from the stronger size dependences from the $\langle k_{\parallel}^2 \rangle$ terms in Eq. (1) in dots. The experimental results lie somewhat lower than the calculations, more so for the dots. We also show in Fig. 3 calculations for zero strain splitting in the quantum well. From comparison with experiment, we see that there is some strain relief, which is consistent with earlier photoluminescence studies on similar structures.²⁰

We have also examined differing treatments of the band coupling to gain insight into their effects. The individual g_e and g_{hh} for quantum dots are given in Fig. 4. Curves K include only conduction-valence-band coupling but no valence-band mixing (“the Kane model”), L include only valence-band mixing (“the Luttinger Hamiltonian”), and those marked K-L include both these couplings. There are significant differences between the curves K-L with all cou-

plings and the simpler K and L treatments. Thus we find that all couplings between the conduction and valence bands and within the valence bands must be included to obtain a quantitative treatment of the g factors. We note that the size dependence of g_{hh} is considerably greater than that of g_e , which is due to the valence-band mixing.

In the present work we have given a full theoretical treatment of Zeeman spin splittings and g factors in semiconductor nanostructures. The results are in good agreement with detailed experimental results for systems with widely varying parameters. They explain key size and magnetic-field dependences in these systems. In addition a perturbation approach is developed for spin splittings in nanostructures which shows in a simple and intuitive way that these size and magnetic-field dependences are intimately connected, and it gives the relationship between these effects in zero-, one-, and two-dimensional systems (quantum dots, wires, and wells). From the analysis here, we see that the effects should be typical of a broad range of nanostructure systems, including quantum dots from self-organized growth for which the

confinement typically is stronger in one direction than in the other two.

We have shown that the Zeeman splitting is given by band coupling in nanostructures. This coupling of spin to electronic and lattice degrees of freedom can play an important role in understanding spin relaxation and spin coherence in nanostructures, which are issues of vital current interest. We have also shown that spin effects can be modified and greatly enhanced in nanostructures. For quantum dots we give the largest enhancements in spin splittings reported to our knowledge, some 20 times greater than the corresponding quantum well values. Such modified and enhanced spin splittings are of considerable interest in connection with the currently active search for implementations for quantum computation, such as those proposed recently for spins in quantum dots^{2,3} and in heterostructures.⁴

This work was supported in part by the U.S. Office of Naval Research, by the Defense Advanced Research Projects Agency, and by the State of Bavaria.

-
- ¹J. M. Kikkawa *et al.*, *Science* **277**, 1284 (1997); J. A. Gupta *et al.*, *Phys. Rev. B* **59**, R10 421 (1999).
- ²A. Imamoglu *et al.*, *Phys. Rev. Lett.* **83**, 4204 (1999).
- ³D. Loss and D. P. DiVincenzo, *Phys. Rev. A* **57**, 120 (1998); G. Burkard *et al.*, *Phys. Rev. B* **59**, 2070 (1999).
- ⁴R. Vrijen *et al.*, *Phys. Rev. A* **62**, 012306 (2000).
- ⁵U. Bockelmann *et al.*, *Phys. Rev. B* **55**, 4469 (1997); W. Heller and U. Bockelmann, *ibid.* **55**, 4871 (1997).
- ⁶D. Gammon *et al.*, *Phys. Rev. Lett.* **76**, 3005 (1996); *Science* **277**, 85 (1997).
- ⁷U. Woggon *et al.*, *Phys. Status Solidi A* **164**, 505 (1997); E. L. Ivchenko, *ibid.* **164**, 487 (1997); S. V. Goupalov and E. L. Ivchenko, *J. Cryst. Growth* **184/185**, 393 (1998).
- ⁸M. Nirmal *et al.*, *Phys. Rev. Lett.* **75**, 3728 (1995); M. Bayer *et al.*, *ibid.* **82**, 1748 (1999).
- ⁹M. J. Snelling *et al.*, *Phys. Rev. B* **45**, 3922 (1992).
- ¹⁰R. J. Warburton *et al.*, *Phys. Rev. B* **43**, 14 124 (1991).
- ¹¹Th. Wimbauer *et al.*, *Phys. Rev. B* **50**, 889 (1994); D. M. Hofmann *et al.*, *ibid.* **55**, 9924 (1997).
- ¹²N. J. Traynor *et al.*, *Phys. Rev. B* **51**, 7361 (1995); N. J. Traynor *et al.*, *ibid.* **55**, 15 701 (1995).
- ¹³E. L. Ivchenko and A. A. Kiselev, *Fiz. Tekh. Poluprovodn.* **26**, 1471 (1992) [*Sov. Phys. Semicond.* **26**, 827 (1992)]; E. L. Ivchenko *et al.*, *Solid State Commun.* **102**, 375 (1997); A. A. Kiselev *et al.*, *Phys. Rev. B* **58**, 16 353 (1998).
- ¹⁴M. Bayer *et al.*, *Phys. Rev. B* **52**, R11 623 (1995).
- ¹⁵Even in high-quality dots grown by self-organized growth the shapes, sizes, and space-dependent alloy concentrations are not yet well known [see N. Liu, J. Tersoff, O. Baklenov, A. L. Holmes, Jr., and C. K. Shih (unpublished)].
- ¹⁶Gerald Bastard, *Wave Mechanics Applied to Semiconductor Heterostructures* (Wiley, New York, 1988), p. 52.
- ¹⁷C. Pidgeon and R. N. Brown, *Phys. Rev.* **146**, 575 (1966).
- ¹⁸The InGaAs/GaAs quantum dot samples used here were similar to those in Ref. 14.
- ¹⁹M. Bayer *et al.*, *Europhys. Lett.* **39**, 453 (1997); *Phys. Rev. B* **57**, 6584 (1998); S. N. Walck and T. L. Reinecke, *ibid.* **57**, 9088 (1998).
- ²⁰R. Steffen *et al.*, *Phys. Rev. B* **54**, 1510 (1996).
- ²¹We have used the following bulk band structure parameters taken from Refs. 10, 12, and 13 and from P. Lawaetz, *Phys. Rev. B* **4**, 3460 (1971) for GaAs and InAs, respectively: the band gap E_g is 1.519 and 0.42 eV, the Kane energy E_p is $2P^2/m_0 = 25.7$ and 22.2 eV with $P = \hbar \langle s | \partial / \partial x | x_i \rangle$, where (s, x_i) are band-edge basis functions with $i = x, y, z$; the spin-orbit coupling parameter Δ is 0.34 and 0.391 eV; the conduction-band effective mass and effective g factor m_c^* and g_c^* are $0.0665m_0$, -0.44 , and $0.023m_0$, -14.99 ; the Luttinger parameters γ_1 , γ_2 , γ_3 , and κ are 7.65, 2.41, 3.28, 1.2 and 19.67, 8.37, 9.29, 7.68. The band gap and the Luttinger parameter κ for $\text{In}_{0.10}\text{Ga}_{0.90}\text{As}$ are 1.370 eV and 1.4, respectively. All other parameters for $\text{In}_{0.10}\text{Ga}_{0.90}\text{As}$ are obtained by averaging the corresponding values for GaAs and InAs. Formulas for the parameters in the present six-band model are given in Ref. 17.
- ²²T. Ando, *J. Phys. Soc. Jpn.* **54**, 1528 (1985).